ACS APPLIED MATERIALS & INTERFACES

Research Article

www.acsami.org

Electrodeposited ZnO—Nanowire/Cu_2O Photovoltaic Device with Highly Resistive ZnO Intermediate Layer

Masanobu Izaki,*[,†] Takayuki Ohta,[†] Misaki Kondo,[†] Toshiaki Takahashi,[†] Fariza Binti Mohamad,[§] Mohd Zamzuri,[†] Junji Sasano,[†] Tsutomu Shinagawa,[‡] and Thierry Pauporté[⊥]

[†]Graduate School of Engineering, Toyohashi University of Technology, Toyohashi, Aichi 441-8580, Japan

[‡]Electronics Materials Department, Osaka Municipal Technical Research Institute, Osaka, 536-8553, Japan

[§]Faculty of Electrical & Electronic Engineering, Universiti Tun Hussein Onn Malaysia, 86400 Parit Raja, Batu Pahat, Johor Malaysia

[⊥]Institut de Recherche de Chimie Paris, CNRS − Chimie ParisTech, UMR8247, 11 rue Pierre et Marie Curie, Paris75005, France

ABSTRACT: Cl-doped ZnO-nanowire (Cl:ZnO-nws)/Cu_2O photovoltaic devices were prepared by electrodeposition in aqueous solutions, and the effects of the insertion of the highly resistive ZnO (i-ZnO) layer has been demonstrated by an improvement of the photovoltaic performance. The Cl:ZnO-nws and i-ZnO layer were prepared by electrodeposition in a zinc chloride aqueous solution with saturated molecular oxygen and simple zinc nitrate aqueous solution, respectively. The i-ZnO layer was directly deposited on the Cl:ZnO-nws and suppressed the electrodeposition of the Cu_2O layer on the Cl:ZnO-nws. The insertion of the i-ZnO layer between the Cl:ZnO-nws and Cu_2O layers induced an improvement in the photovoltaic performance from 0.40 to 1.26% with a 0.35 V open circuit voltage, 7.1 $mA{\cdot}cm^{-2}$ short circuit current density, and 0.52 fill factor due to the reduction of the recombination loss.

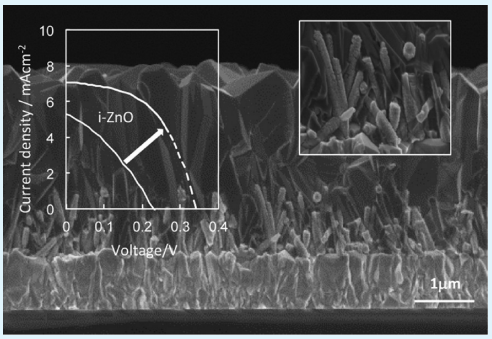

KEYWORDS: *zinc oxide, cuprous oxide, nanowire, electrodeposition, photovoltaic device*

1. INTRODUCTION

Cuprous oxide (Cu_2O) is a p-type semiconductor with the band-gap energy of 2.1 eV[1] and has attracted increasing attention as a light-absorbing layer in a photovoltaic device, because of its nontoxicity, abundance, and theoretical conversion efficiency of 18%. The Cu_2O layer for photovoltaic applications has been prepared by the thermal oxidation of a metallic Cu sheet in air at 1273 K,[2] sputtering,[3] and electrodeposition in an aqueous solution.[4] The conversion efficiency of 5.38% has been reported for a photovoltaic device with the Cu_2O layer prepared by thermal oxidation with ZnO and Ga_2O_3 layers prepared by a pulse-laser deposition technique.[5] In contrast, solution chemical processes, including the electrodeposition, have several advantages over the thermal ones, and the conversion efficiencies of 3.97 and 2.85% have been reported for the electrodeposited Cu_2O photovoltaic devices with Ga_2O_3 and ZnO layers prepared by an atomic layer deposition.[6,7] The conversion efficiency, however, is limited, up to now, to 1.28% for the ZnO/Cu_2O photovoltaic device prepared only by electrodeposition.[4] The mobility of the majority carrier was reported to be 1.2 $cm^2{\cdot}V^{-1}{\cdot}s^{-1}$ for the electrodeposited Cu_2O layer,[8] and the value was much lower than 90 $cm^2{\cdot}V^{-1}{\cdot}s^{-1}$ reported for the thermally oxidized Cu_2O layer.[9] Since the diffusion length of the generated carriers by light irradiation is a function of the mobility and relaxation time, the active region to generate the carrier in the Cu_2O layer is limited to the region near the heterointerface with the ZnO layer. Musselman and co-workers have shown the advantage of using ZnO nanowires to expand the active region around the ZnO-nws.[10] Moreover, electrodeposited Cl-doped ZnO-nws (Cl:ZnO-nws) can be used for this purpose due to its low resistivity.[11] The low resistivity originates from the Cl impurity incorporated in the ZnO semiconductor;[12] however, the impurities present near the heterointerface act as recombination sites, resulting in a decrease in the photovoltaic performance. It has been demonstrated that the recombination loss is strongly reduced by inserting a highly resistive ZnO layer between the n-ZnO and phthalocyanine layers in the layered hybrid photovoltaic device.[13]

Here, we show the preparation of a Cl:ZnO-nws/Cu_2O photovoltaic device by electrodeposition in aqueous solutions and effects of the insertion of the highly resistive ZnO (i-ZnO) layer on the photovoltaic performance. The Cl:ZnO-nws and i-ZnO layer were prepared in a zinc chloride aqueous solution saturated with a molecular oxygen precursor and a simple zinc nitrate aqueous solution, respectively. The i-ZnO layer was directly deposited on the Cl:ZnO-nws and suppressed the deposition of the Cu_2O layer on the Cl:ZnO-nws. They favored a bottom-up growth, starting from the near F-doped SnO_2-coated glass substrate (FTO) region. The insertion of the i-

Received: April 14, 2014
Accepted: July 31, 2014
Published: July 31, 2014

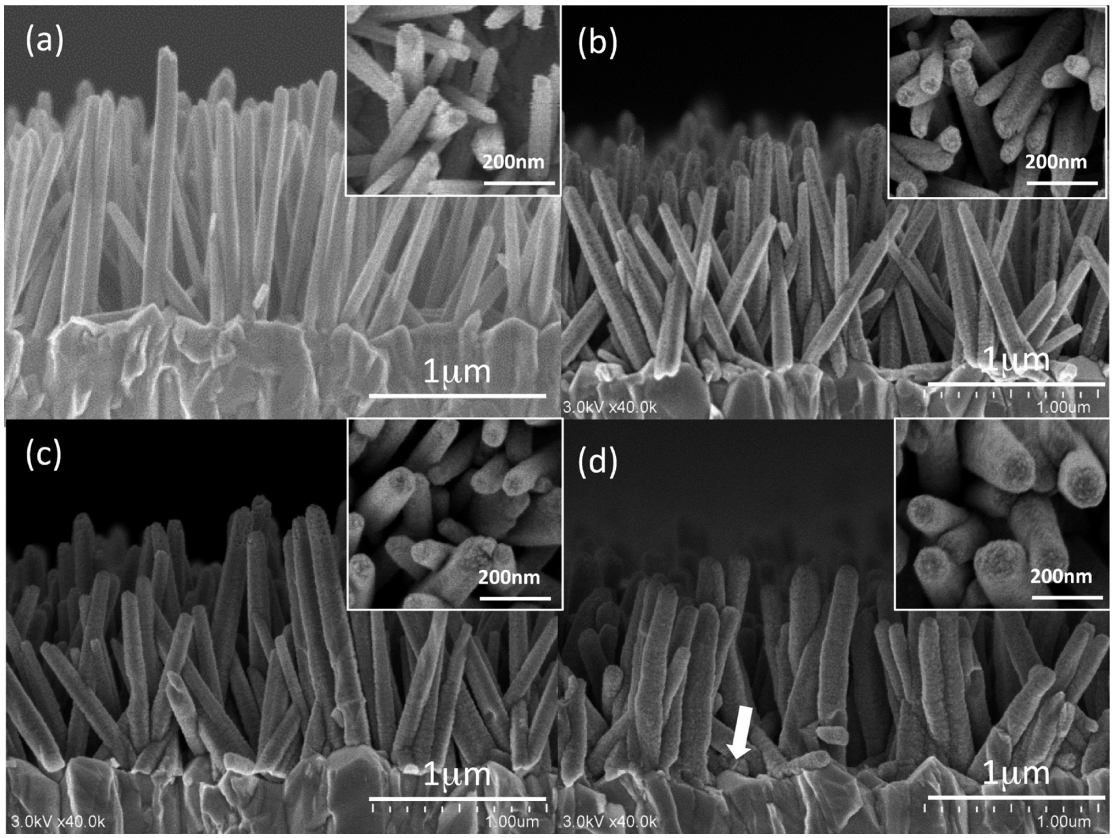

Figure 1. Cross-sectional structures and surface morphology (inset) of Cl-doped ZnO nanowires (a) before and after coating with highly resistive i-ZnO layer for (b) 5 s, (c) 10 s, and (d) 20 s.

ZnO between the Cl:ZnO-nws and Cu_2O layers induced an improvement in the conversion efficiency from 0.40 to 1.26%.

2. EXPERIMENTAL SECTION

The Cl:ZnO-nws layer was prepared on an FTO substrate (AGC Fabritech Co., Ltd., Type DU) by electrodeposition in an aqueous solution containing 0.2 mmol/L zinc chloride hydrate and 0.1 mol/L KCl at 353 K using a potentiostat (AUTOLAB PGSTAT30).[14] The solution was saturated with molecular oxygen, and O_2 bubbling was maintained during the electrodeposition.[15] The FTO substrate was fixed and connected to a rotating disk electrode (RDE), and the rotation was carried out at a constant rotation speed of 300 rpm.[16] The electrodeposition was performed for 3600 s in a three-electrode cell at a potential of −1.0 V referenced to the saturated calomel electrode (SCE). The i-ZnO layer was prepared by electrodeposition at −1.0 to −1.2 V referenced to a Ag/AgCl electrode for 5−20 s in an aqueous solution containing 0.08 mol/L zinc nitrate hydrate[17] at 333 K using a potentiostat (Hokuto Denko, HA-501) connected to a coulomb meter (Hokuto Denko, HF-201). The Cu_2O layer was prepared by electrodeposition at 313 K in an aqueous solution containing a 0.4 mol/L copper(II) acetate hydrate and 3 mol/L lactic acid. The solution pH was adjusted to 12.5 with a KOH aqueous solution. The electrodeposition was carried out at −0.4 V referenced to a Ag/AgCl electrode using a potentiostat (Hokuto Denko, HABF-501A). The solutions were prepared with reagent-grade chemicals and distilled water purified by a Millipore Elix Advantage system.

Before the electrodeposition of the Cl:ZnO-nws, the FTO substrate was successively cleaned in acetone and ethanol for 6 min each in an ultrasonic bath. These FTO substrates were immersed in an HNO_3 aqueous solution for 2 min, rinsed with distilled water, and then used for the experiment. After the Cu_2O deposition, a Au electrode with a size of 3 mm × 3 mm was deposited on top of the Cu_2O layer by vacuum evaporation (ULVAC, VPC-260F system).

An X-ray photoelectron spectroscopy (XPS) analysis was performed using an ULVAC-PHI Model 5700MC with monochromated Al Kα radiation at a pressure of around 1.6×10^{-8} Pa. Binding energies were corrected by referencing the C 1s signal of the adventitious contamination hydrocarbon to 284.8 eV. The electron pass energy in the analyzer was set at 11.75 eV corresponding to 0.57 eV of full width at half-maximum (fwhm) of the Ag 3d5/2 peak at 368.35 eV. The Ar sputtering was carried out for 1 min at 1 kV by a differential pumping type ion etching gun. The X-ray diffraction patterns were recorded by a $\theta/2\theta$ scanning technique with monochromated Cu Kα radiation operated at 40KV and 200 mA using a Rigaku RINT2500. The optical absorption spectra were measured using a UV−vis−near-infrared spectrophotometer (Hitachi, U4100) with reference to the bare substrate. Electron microscopy observations were carried out using a field-emission scanning electron microscope (FE-SEM, Hitachi, SU8000). The electrical characterization was carried out by the van der Pauw method using a Hall effect measuring system (Toyo Technica, Resitest 8310) in air at ambient temperature and 0.3 T magnetic field. The samples were prepared by mechanically splitting them off from the glass substrate followed by fastening in epoxy resin (Araldite 2091). Four In electrodes were prepared on the ZnO samples using the vacuum evaporation system. The electrical characteristic was estimated by recording the current density−voltage curves in dark and under AM1.5G illumination with a 100 mW·cm^{-2} power (Bunko Keiki, OTENTO-SUN III solar simulator system) by a Keithley 2400 source meter.

3. RESULTS AND DISCUSSION

Figure 1 shows FE-SEM images of the side and top surface of the Cl:ZnO-nws before and after the electrodeposition of i-ZnO for 5, 10, and 20 s. The Cl:ZnO-nws grew straight from the FTO substrate, and the bare surface of the FTO substrate could be observed between the Cl:ZnO-nws. The mean length

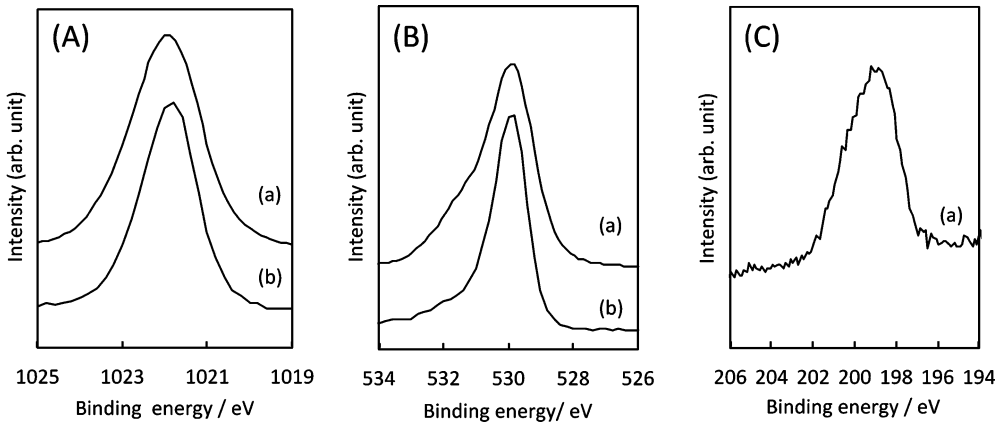

Figure 2. (A) Zn 2p, (B) O 1s, and (C) Cl 2p electron spectra for Cl-doped ZnO nanowires (a) before and (b) after electrodeposition of the i-ZnO layer for 20 s.

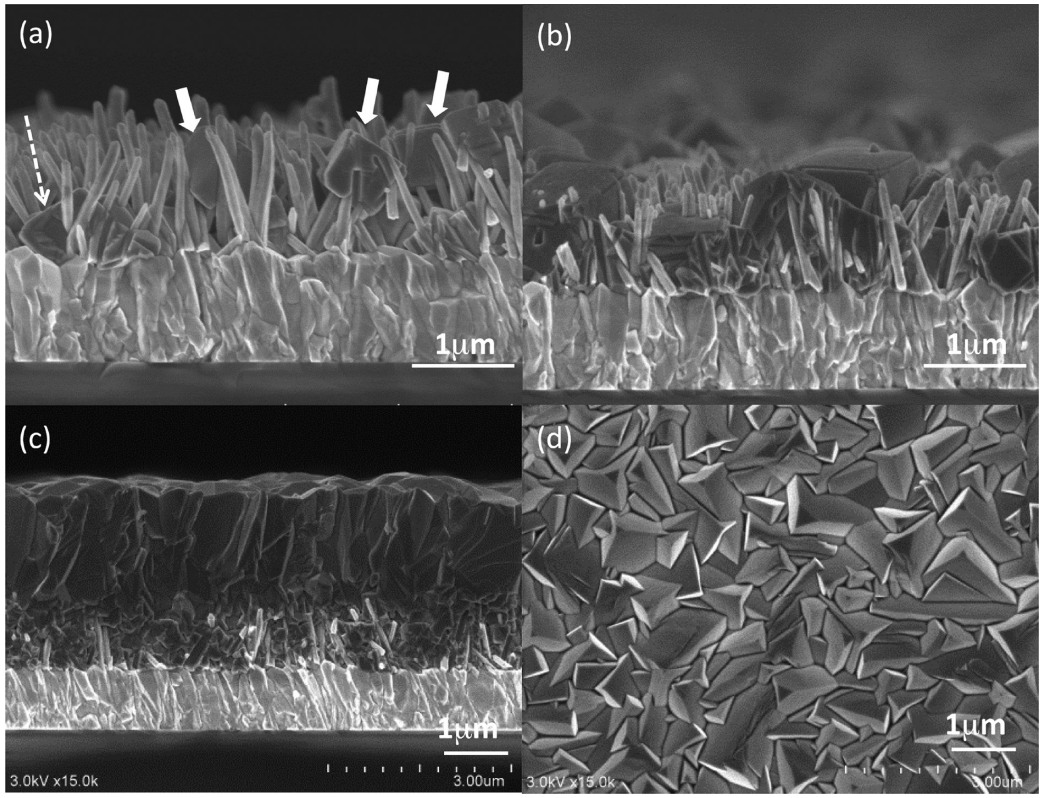

Figure 3. Cross-sectional structures of Cu_20 layers deposited on Cl-doped ZnO nanowires for electric charges of (a) 0.4, (b) 0.65, and (c) 1.7 C·cm^{-2}. (d) The surface morphology of the Cu_20 layer.

and width of the Cl:ZnO-nws were estimated to be 1.13 μm and 85 nm, respectively, and the hexagonal facets corresponding to the (0001) planes could be observed on the top views.[18] The ZnO nuclei deposited during the initial stage of the growth possessed a random orientation due to the random orientation of the SnO_2 polycrystalline layer of the FTO substrate, and then the ZnO nuclei grew in the direction of the ⟨0001⟩ orientation due to the lowest surface energy in the wurtzite structure, resulting in the formation of tilted Cl:ZnO-nws.[19] Both the side and top surfaces of the Cl:ZnO-nws were very smooth.

The electrodeposition of the i-ZnO for the deposition time of 5 to 20 s did not affect the length and orientation of the Cl:ZnO-nws. Isolated small grains of approximately 15.5 nm in size could be observed on both the side and top surfaces of the Cl:ZnO-nws after the electrodeposition for 5 s, and after 20 s, the grains with a size of approximately 22.5 nm were deposited over the entire side and top surfaces of the Cl:ZnO-nws (Figure 1d). The width of the Cl:ZnO-nws increased with an increase in the deposition time and was estimated to be 102, 120, and 149 nm at 0, 5, 10, and 20 s, respectively. The thickness of the i-ZnO layer calculated from the difference in the wire width before and after the electrodeposition of i-ZnO was 8.5, 17, and 32 nm for 5, 10, and 20 s, respectively. The thickness (d, nm) linearly varied with the deposition time (t, s) according to $d = 1.67t$. The thickness of the i-ZnO layer was smaller than the grain size for the deposition times shorter than 10 s. This suggests the imperfect coverage of Cl:ZnO-nws with the i-ZnO

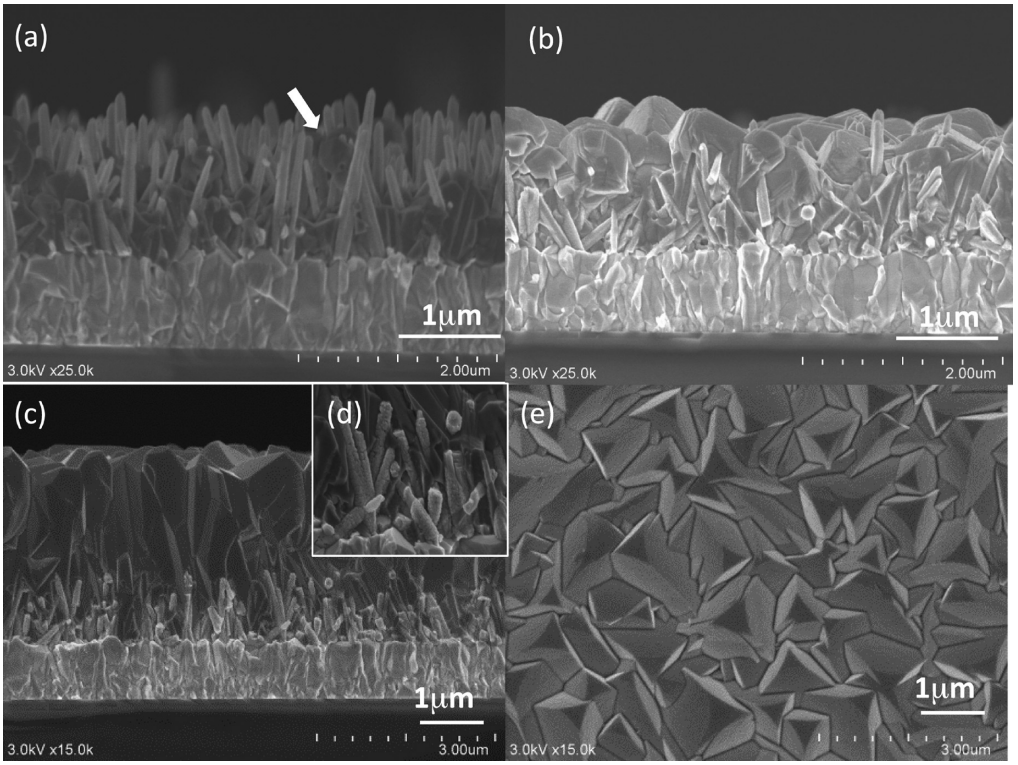

Figure 4. Cross-sectional structures of Cu_2O layers deposited on Cl-doped ZnO nanowires/i-ZnO for electric charges of (a) 0.4, (b) 0.65, and (c, d) 1.7 $C \cdot cm^{-2}$. (e) The surface morphology of the Cu_20 layer.

grains. It was difficult to confirm the deposition of the i-ZnO layer on the FTO substrate based on the FE-SEM views, although the contrast change on the FTO surface could be partly seen after 20 s, as denoted by the arrows in Figure 1d.

Figure 2 shows the Zn 2p, O 1s, and Cl 2p electron spectra for the Cl:ZnO-nws before and after the electrodeposition of the i-ZnO layer for 20 s. The escaping depth of an electron was approximately 3−4 monolayers due to the electron energy ranging from 194 to 1026 eV. The incident Al Ka radiation was irradiated at an angle of 45° in the direction normal to the sample surface, and the hemispherical analyzer was set at a direction normal to the sample surface. The electron spectra recorded here reflected the region near the top surface of the Cl:ZnO-nws with and without the i-ZnO layer. Both Zn 2p spectra showed a peak at the binding energy of 1022 eV, which corresponded to the Zn^{2+} state in ZnO.[20]

The bare Cl:ZnO-nws showed a shoulder at ∼531.2 eV in addition to the peak at 530 eV. The O^{2-} state in ZnO and the OH^- state in $Zn(OH)_2$ possessed binding energies of 530 and 531.2 eV, respectively.[19] The shoulder at 531.2 eV decreased by depositing the i-ZnO layer for 20 s, while keeping the peak energy at 530 eV. The Ar sputtering was carried out to remove the surface contamination of the Cl:ZnO-nws using an ion etching gun prior to the measurements. Since the ion etching gun was placed in the analyzer chamber in a direction different from the incident X-ray source and analyzer, it was impossible to perfectly remove the surface contamination including $Zn(OH)_2$.

The bare Cl:ZnO-nws showed a peak at 199 eV on the Cl 2p electron spectrum, and the energy agreed with that for the Cl^- state in $ZnCl_2$.[21] The compound of ClO_4^- was reported to have a binding energy of around 208 eV.[20] The existence of the Cl 2p peak at 199 eV suggested that the Cl impurity incorporated into the ZnO was bound to the Zn cation. The Cl content calculated using the sensitivity factor[20] was estimated to be approximately 1% for the bare Cl:ZnO-nws. Also, the Cl content can be controlled by adjusting the preparation conditions such as the solution formulation, current density, and solution temperature.[12] The Cl 2p peak disappeared by depositing the i-ZnO layer for 20 s.

Figure 3 shows cross-sectional views of the Cu_2O layers directly deposited on the Cl:ZnO-nws for electric charges of 0.4, 0.65, and 1.7 $C \cdot cm^{-2}$ and the surface morphology of the resultant Cu_2O layer. After 0.4 $C \cdot cm^{-2}$ of an electrical charge was exchanged, most of the cubic-shaped Cu_2O grains with a size of 0.4−0.6 μm were directly grown on the Cl:ZnO-nws, away from the FTO substrate. Therefore, the Cl:ZnO-nws were embedded inside the Cu_2O, as denoted by the white arrows in Figure 3a. Some Cu_2O grains were directly deposited on the FTO substrate, but the bare surface of the FTO substrate could be clearly observed between the Cl:ZnO-nws.

The Cu_2O layer deposited for 0.65 $C \cdot cm^{-2}$ was a heterogeneous mixture of two types of grains and possessed an irregular surface due to the existence of the top edge of the Cl:ZnO-nws and of the flat surface of large Cu_2O grains (Figure 3b). Cu_2O grains with the size of 0.5−0.6 μm could be observed near the substrate, and some Cl:ZnO-nws were embedded in the Cu_2O grains, resulting from the growth of Cu_2O grains deposited on the FTO substrate at 0.4 $C \cdot cm^{-2}$. Moreover, large cubic Cu_2O grains with a size over 1.2 μm were separately observed on the layer's outer part and originated from the Cu_2O grains deposited on the Cl:ZnO-nws. The Cl:ZnO-nws were embedded inside the Cu_2O layer, and no damage, such as fracture, could be observed. However, bare surface areas of the FTO substrate were still observed between the Cu_2O grains.

A continuous Cu_2O layer with a thickness of 3.3 μm was formed at 1.7 C·cm^{-2}, and the surface was very smooth (Figure 3c,d). No defects, such as pores, could be found throughout the layer thickness, and the space observed between the Cu_2O grains at 0.65 C·cm^{-2} disappeared, filled with the Cu_2O grains. The Cu_2O layer was composed of a mixture of granular crystallites with a size of ~0.3 μm and upper columnar grains of ~2 μm in length and 1 μm in width. The small Cu_2O crystallites were observed at a thickness below approximately 1.3 μm corresponding to the length of the Cl:ZnO-nws. The columnar Cu_2O grains were formed at a thickness over 1.3 μm and grew in the direction normal to the surface. The surface of the resultant Cu_2O layer was composed of aggregated angular grains with a size of approximately 1.0 μm, and no defects, such as pores, could be observed on the surface (Figure 3d).

Figure 4 shows the cross-sectional structures of the Cu_2O layers deposited on the Cl:ZnO-nws/i-ZnO for the electric charges of 0.4, 0.65, and 1.7 C·cm^{-2} and the surface morphology of the resultant Cu_2O layer. The i-ZnO layer was deposited at −1.1 V for 20 s. Almost all the Cu_2O grains with a size of approximately 0.35 μm were directly deposited on the FTO substrate, and the Cu_2O grains deposited on the Cl:ZnO-nws/i-ZnO was rarely observed, as denoted by the white arrows in Figure 4a. The surface of the FTO substrate between the Cl:ZnO-nws/i-ZnO was covered with the deposited Cu_2O grains. No change in the length and width of the Cl:ZnO-nws could be observed before and after the Cu_2O deposition. After 0.65 C·cm^{-2} of electric charge exchanged (Figure 4b), the Cu_2O grains embedded the Cl:ZnO-nws/i-ZnO, and the space between the Cl:ZnO-nws/i-ZnO was perfectly filled by the Cu_2O phase. Defects, such as pores, were not observed throughout the Cu_2O layer. For an electric charge exchange of 1.7 C·cm^{-2} (Figure 4c−e), the Cu_2O layer was composed of aggregated columnar Cu_2O grains grown in direction normal to the surface. No defects, such as pores, were observed throughout the layer thickness. The thickness of the Cu_2O layer was estimated to be approximately 1.4 μm (0.65 C·cm^{-2}) and 3.3 μm (1.7 C·cm^{-2}) corresponding to the value theoretically calculated from the electric charge with the assumption of a 100% current efficiency. The surface of the resultant Cu_2O layer was composed of aggregates of angular grains without any pores (Figure 4e). Also, small i-ZnO grains could be observed on the Cl:ZnO-nws even after the Cu_2O electrodeposition (Figure 4d).

The electrodeposition of the i-ZnO layer induced the suppression of the Cu_2O deposition on the Cl:ZnO-nws and the preferential bottom-up growth starting from the FTO substrate. This resulted in the formation of the Cu_2O layer embedding the Cl:ZnO-nws/i-ZnO. The cathodic electrodeposition of the Cu_2O layer from the alkaline aqueous solution containing the cupric lactate complex is described as follows:[22]

$$Cu^{2+} + 2L^- \rightarrow [Cu^{II}{-}L_2] \quad (1)$$

with $[Cu^{II}{-}L_2]$:cupric lactate complex

$$[Cu^{II}{-}L_2] + e^- \rightarrow Cu^+ + 2L^- \quad (2)$$

$$Cu^+ + OH^- \rightarrow [Cu^{I}OH] \quad (3)$$

$$2[Cu^{I}OH] \rightarrow Cu_2O + H_2O \quad (4)$$

The electrons needed for the formation of the Cu_2O deposition were supplied from both the FTO substrate and Cl:ZnO-nws, and the supplement from the Cl:ZnO-nws was suppressed by the i-ZnO layer. The Cl:ZnO-nws contained a certain amount of a Cl^- impurity originating from the zinc chloride and potassium chloride in the solution, and the Cl^- impurity acted as a donor in the ZnO semiconductor.[23] The continuous Cl:ZnO layer prepared from a 5 mmol/L zinc chloride solution with a saturated molecular oxygen was electrically characterized with the van der Pauw method and showed a resistivity of 4.4×10^{-2} Ω·cm with a 1.5×10^{19} cm^{-3} carrier concentration and a mobility of 9.57 cm^2·V^{-1}·s^{-1}. The carrier concentration nearly agreed with 6.2×10^{19} cm^{-3} reported for the Cl:ZnO-nws prepared in the same manner.[24] The resistivity on the order of 10^8 Ω·cm was obtained for the 1 μm thick i-ZnO layer prepared at −1.1 V by the van der Pauw method; however, the carrier concentration and mobility could not be estimated because of the high layer resistivity originating from the small grain size and defects incorporated into the ZnO layer.[25] The change in the growth of the electrodeposited Cu_2O layer by the insertion of the i-ZnO layer was attributed to the high resistivity of the i-ZnO layers. The bottom-up growth was reported for the Cu_2O electrodeposition on ZnO-nanorods and for the ZnO seed layer prepared in a zinc nitrate aqueous solution used for the preparation of the i-ZnO layer.[26]

Figure 5 shows X-ray diffraction patterns for Cl:ZnO-nws, Cl:ZnO-nws/i-ZnO, and Cl:ZnO-nws/i-ZnO/Cu_2O. The X-ray

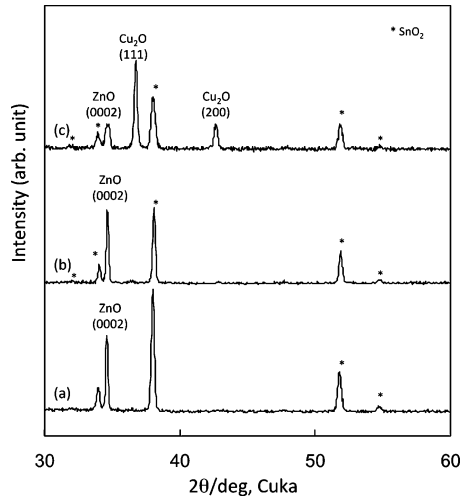

Figure 5. X-ray diffraction patterns of (a) Cl-doped ZnO nanowire, (b) Cl-doped ZnO nanowire/i-ZnO, and (c) Cl-doped ZnO nanowire/i-ZnO/Cu_20 structures.

diffraction patterns for the i-ZnO/ZnO-nws and Cu_2O/i-ZnO/ZnO-nws structures were almost the same in profile and peak angles, irrespective of the deposition time of the i-ZnO. The Cl:ZnO-nws showed only one peak assigned to the reflection of the (0002) planes of the wurtzite ZnO crystal[27] in addition to those originating from the SnO_2[28] of the FTO substrate, indicating the formation of a (0001) preferred orientation. The electrodeposition of the i-ZnO layer had no effect on the intensity and angles of the diffraction X-ray pattern due to the thinness. The electrodeposition of the Cu_2O layer added two peaks assigned to the (111) and (200) planes of Cu_2O that are characteristic of the cubic cupric lattice[29] in addition to those originating from the ZnO and SnO_2. The X-ray diffraction pattern of the Cu_2O layer was almost the same in peak intensity and angle irrespective of the existence of the i-ZnO layer and

electric charge of the Cu_2O deposition. The Cu_2O layer possessed a slight (111) preferred orientation from the peak intensity ratio compared to that tabulated on the International Centre for Diffraction Data (ICDD) card[21] and almost agreed with that of a Cu_2O layer prepared on a two-dimensional continuous ZnO layer.[1] The lattice constant calculated from the peak angles was estimated at 0.4234 nm, which is smaller than 0.4269 nm listed on the ICDD card[29] and 0.4261 nm for an unconstrained Cu_2O layer prepared on the continuous ZnO layer.[1] We note that the strain-induced lattice parameter changes have been previously described, for instance, in the case of a nanoporous ZnO layer electrodeposited between arrayed ZnO-nws.[30]

Figure 6 shows the correlation between the light absorption coefficient and photon energy for the Cl:ZnO-nws, Cl:ZnO-nws/i-ZnO, and Cu_2O layer prepared on the Cl:ZnO-nws/i-ZnO. The band-gap energy was estimated by extrapolating the linear part with the assumption of a direct optical transition for both ZnO and Cu_2O. The band-gap energy was 3.31 eV for the Cl:ZnO-nws and changed to 3.26 eV after deposition of the i-ZnO layer. These values were consistent with those already reported for the Cl:ZnO-nws and i-ZnO layer.[24] The band-gap energy was estimated to be 2.02 eV for the Cu_2O layer, irrespective of the electric charge.

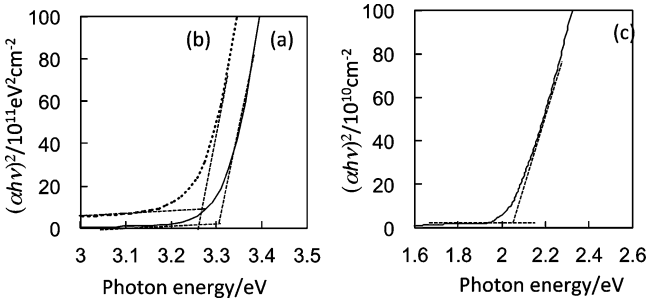

Figure 6. Correlations between absorption coefficient and photon energy for Cl-doped ZnO nanowire (a) before and after electrodeposition of i-ZnO layer for (b) 20 s, and (c) Cu_20 layer.

Figure 7 shows the current density–voltage curves of the Cl:ZnO-nws/Cu_2O photovoltaic (PV) devices prepared with and without the i-ZnO layer. All the Cl:ZnO-nws/Cu_2O PV devices generated electricity under the AM1.5G illumination. The i-ZnO-free Cl:ZnO-nws/Cu_2O PV device showed a conversion efficiency of 0.40% with a 0.23 V open circuit voltage (V_{oc}), 5.3 mA·cm^{-2} short circuit current density (J_{sc}), and 0.33 fill factor (FF). The performance was nearly close to 0.47% already reported for the PV devices prepared in a similar manner.[31] The insertion of the i-ZnO layer induced an improvement in the photovoltaic performance. The V_{oc} and FF were improved by the increasing deposition time, and the maximum values of 0.34 and 0.52 V were obtained for 20 s. J_{sc} increased to 7.56 mA·cm^{-2} with increasing the deposition time at 10 s and then slightly decreased to 7.09 mA·cm^{-2} for 20 s. The conversion efficiency was improved with the increasing deposition time, and the maximum conversion efficiency of 1.26% was achieved for 20 s. As discussed earlier, the thickness of the i-ZnO layer was linearly proportional to the deposition time. The grain size of the i-ZnO layer deposited on the Cl:ZnO-nws ranged from 15 to 23 nm, and the thickness was smaller than the grain size for deposition times below 10 s. This comparison suggests a noncontinuous i-ZnO layer with separated grains deposited on the Cl:ZnO-nws and the existence of an exposed area of Cl:ZnO-nws between the i-ZnO grains. However, the exact morphology of the surface could not be determined by the FE-SEM imaging. The defects located at the surface of the Cl:ZnO-nws act as recombination sites,[32] resulting in a decreased photovoltaic performance. A deposition time of 20 s was needed to cover all the surface of the Cl:ZnO-nws with the i-ZnO layer. The electrodeposition of Cu_2O grains preferentially occurred on the FTO substrate at 20 s for the i-ZnO deposition, and a continuous Cu_2O layer could be formed by the growth. Although the formation of the i-ZnO layer could not be confirmed by the FE-SEM observation, the improvement in the photovoltaic performance indicated that the deposited i-ZnO layer suppressed the electrical shorting between the Cu_2O layer and FTO substrate.

Figure 8 shows the effects of the deposition potential of the i-ZnO layer on the photovoltaic performance of Cl:ZnO-nws/i-ZnO/Cu_2O PV devices. The deposition time was fixed at 20 s. The maximum conversion efficiency of 1.26% was achieved at −1.1 V, and all the photovoltaic parameters decreased at both −1.0 and −1.2 V. The electrical properties of resistivity, carrier concentration, and mobility changed depending on the preparation conditions of the cathodic potential and current density for the electrodeposited ZnO layers.[25] The i-ZnO layers prepared at a potential ranging from −1.0 to −1.2 V possessed a very high resistivity on the order of 10^8 Ω·cm, with an unknown carrier concentration. It is speculated from the results already reported on the electrical characteristics that the carrier concentration is on the order of 10^{11} cm^{-3} ($N_{c,i\text{-}ZnO}$) and decreased with the shift in the potential to the negative side.[25] The carrier concentration of the Cl:ZnO-nws was 1.5×10^{19} cm^{-3} ($N_{c,Cl:ZnO\text{-}nws}$) as already estimated in this study.

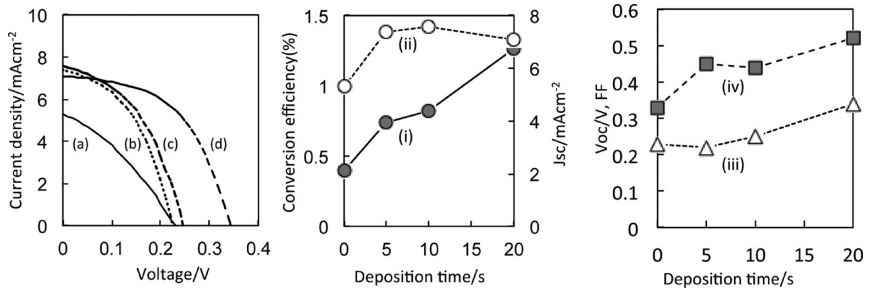

Figure 7. Current density–voltage curves for Cl-doped ZnO nanowire/Cu_2O photovoltaic devices with i-ZnO layers deposited for (a) 0, (b) 5, (c) 10, and (d) 20 s, and the relation of (i) conversion efficiency, (ii) short circuit current density (J_{sc}), (iii) open circuit voltage (V_{oc}), and (iv) FF to the deposition time.

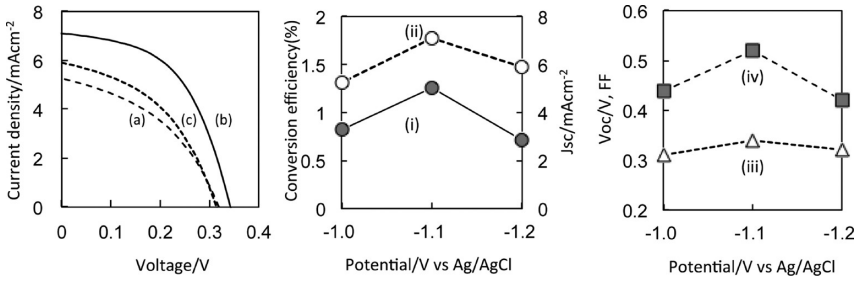

Figure 8. Current density−voltage curves for Cl-doped ZnO nanowire/Cu_2O photovoltaic devices with i-ZnO layers deposited at (a) −1.0, (b) −1.1, and (c) −1.2 V, and the relation of (i) conversion efficiency, (ii) short circuit current density(J_{sc}), (iii)open circuit voltage (V_{oc}), and (iv) FF to the potential.

The location of the Fermi level (E_F) is closely related to the carrier concentration. The energy difference (ΔE_c) between the conduction band energy minimum (CBM) and Fermi level (E_F) is estimated for n-type semiconductors by the following equation:[33]

$$\Delta E_c = \mathrm{CBM} - E_F = kT \log_e(N_c/n) \quad (5)$$

where k, T, and N_c are the Boltzmann constant, temperature, and effective density of state in the conduction band. The energy difference (ΔE_c) decreased with increasing the carrier concentration corresponding to the donor density until the donor density reached the effective density of state (N_c). The energy differences for i-ZnO ($\Delta E_{c,i\text{-}ZnO}$) and Cl:ZnO-nws ($\Delta E_{c,Cl:ZnO\text{-}nws}$) were calculated according to eq 5, and the difference of $\Delta E_{c,i\text{-}ZnO} - \Delta E_{c,Cl:ZnO\text{-}nws}$ could be calculated to be approximately 0.5 eV.

The energy difference (ΔE_v) between the valence band maximum (VBM) and Fermi level (E_F) could be estimated for the p-Cu_2O layer by the following equation:[33]

$$\Delta E_v = E_F - \mathrm{VBM} = kT \log_e(N_V/p) \quad (6)$$

The carrier concentration (p) corresponding to the acceptor density was reported to be 1.9×10^{14} cm^{-3} for a Cu_2O layer prepared in the same manner.[1] The energy difference (ΔE_v) was calculated to be approximately 0.3 eV with the assumption for the effective density of state in the valence band (N_V) to be on the order of 10^{19} cm^{-3}.

A cliff-type conduction band offset[34] was formed at the heterointerface between the Cl:ZnO-nws and Cu_2O layer, and the defects that originated from the high carrier concentration act as a recombination site[32] near the interface. The i-ZnO layer possessed a Fermi level lower by approximately 0.5 eV than that for the Cl:ZnO-nws, and the concentration of defects, which act as a donor in the ZnO semiconductor, was relatively low. The insertion of the i-ZnO layer between the Cl:ZnO-nws and Cu_2O layer could play a role in suppressing the recombination loss due to the decrease in the conduction band offset and increase in the depletion layer. Moreover, the observed change in the photovoltaic performance with the i-ZnO deposition cathodic potential indicates the importance of the value of the conduction band offset, which is determined by the ionization energy as demonstrated for Cu(InGa)Se_2/Zn(OS)/ZnO solar cells.[34] The change in the carrier concentration somewhat affects the ionization energy, but further investigation with an inverse photoemission spectroscopy is needed to accurately illustrate the conduction band offset at the heterointerface.

The continuous ZnO layer/Cu_2O PV devices prepared only by electrodeposition showed the best conversion efficiency of 1.28% with a 0.59 V in V_{oc}, 3.8 mA·cm^{-2} in J_{sc}, and 0.58 in FF.[4] The use of the Cl:ZnO-nws alternative to the continuous ZnO layer produced a major improvement in the J_{sc} from 3.8 to 7.56 mA·cm^{-2} due to the increase in the active region expanded along the Cl:ZnO-nws, but the V_{oc} decreased from 0.59 V[4] to 0.35 V. This suggested the imperfect control of the quality of the i-ZnO layer, such as the homogeneity, thickness, and electrical characteristics.

The maximum conversion efficiency of 5.38% has been reported for an Al-doped ZnO(AZO)/Ga_2O_3/Cu_2O PV device prepared by the thermal oxidation of a metallic Cu sheet followed by a pulse-laser deposition of Ga_2O_3 and AZO layers.[5] The V_{oc} changed from 0.55 to 0.80 V depending on the oxide material inserted between the Cu_2O and AZO layers,[35,36] and the best value was achieved with a Ga_2O_3 buffer layer. Also, a 1.2 V V_{oc} has been reported for the electrodeposited Cu_2O photovoltaic device with Ga_2O_3 prepared by an atomic layer deposition.[6] The J_{sc} value obtained in this study was slightly lower than that for the AZO/Ga_2O_3/Cu_2O PV device, and the V_{oc} was half that for the AZO/Ga_2O_3/Cu_2O PV device. Further investigation on controlling the heterointerface state and the electrical property of the Cu_2O layer is indispensable for improving the photovoltaic performance.

4. CONCLUSIONS

Cl-doped ZnO-nanowire (Cl:ZnO-nws)/Cu_2O photovoltaic (PV) devices have been prepared by electrodeposition, and the effects of the insertion of a highly resistive ZnO layer (i-ZnO) on the photovoltaic performances has been investigated. The Cl:ZnO-nws and i-ZnO layer were prepared in a zinc chloride aqueous solution with saturated molecular oxygen and in a zinc nitrate aqueous solution, respectively. The Cu_2O layer was prepared in an alkaline aqueous solution containing a copper(II) acetate hydrate and lactic acid. The i-ZnO grains were directly deposited on the Cl:ZnO-nws, and the thickness increased with the increasing deposition time. The direct deposition of the Cu_2O layer on the Cl:ZnO-nws was suppressed by the deposited i-ZnO layer with a high resistivity. The insertion of the i-ZnO layer between the Cl:ZnO-nws and Cu_2O layer produced an improvement in the photovoltaic performance depending on the deposition potential and time. The conversion efficiency was boosted from 0.40 to 1.26% by inserting the i-ZnO layer prepared at −1.1 V for 20 s due to the reduction in the recombination loss at the heterointerface. These results reveal the importance of the heterointerface state and the possibility for oxide-based photovoltaic devices to be the next generation of thin film solar cells.

AUTHOR INFORMATION

Corresponding Author

*E-mail: m-izaki@me.tut.ac.jp.

Notes

The authors declare no competing financial interest.

ACKNOWLEDGMENTS

This work was supported in part by the Incorporated Agency New Energy and Industrial Development Organization (NEDO) under the Japanese Ministry of Economy, Trade, and Industry (METI), a Grant-in-Aid for Scientific Research (25281062), and Japan-France Integrated Action Program (SAKURA) under the Japan Society of the Promotion of Science (JSPS), and Amano Industrial Research Institute Foundation.

REFERENCES

(1) Mizuno, K.; Izaki, M.; Murase, K.; Shinagawa, T.; Chigane, M.; Inaba, M.; Tasaka, A.; Awakura, Y. Structural and Electrical Characterizations of Electrodeposited P-Type Semiconductor Cu_2O Films. *J. Electrochem. Soc.* **2005**, *152*, C179−C182.

(2) Mittiga, A.; Salza, E.; Sarto, F.; Tucci, M.; Vasanthi, R. Heterojunction Solar Cell with 2% Efficiency Based on a Cu_2O Substrate. *Appl. Phys. Lett.* **2006**, *88*, 163502/1−163502/2.

(3) Paul, G. K.; Ghosh, R.; Bera, S. K.; Bandyopadhyay, S.; Sakurai, T.; Akimoto, K. Deep Level Transient Spectroscopy of Cyanide Treated Polycrystalline p-Cu_2O/n-ZnO Solar Cell. *Chem. Phys. Lett.* **2008**, *463*, 117−120.

(4) Izaki, M.; Shinagawa, T.; Mizuno, K.; Ida, Y.; Inaba, M.; Tasaka, A. Electrochemically Constructed P-Cu_2O/n-ZnO Heterojunction Diode for Photovolatic Device. *J. Phys. D: Appl. Phys.* **2007**, *40*, 3326−3329.

(5) Minami, T.; Nishi, Y.; Miyata, T. High-Efficiency Cu_2O-Based Heterojunction Solar Cells Fabricated using a Ga_2O_3 Thin Film as N-Type Layer. *Appl. Phys. Express* **2013**, *6*, 4101/1−044101/4.

(6) Lee, Y. S.; Chuo, D.; Brandt, R. E.; Siah, S. C.; Li, J. V.; Mailoa, J. P.; Lee, S. W.; Gordon, R. Y.; Buonassisi, T. Atomic Layer Deposited Gallium Oxide Buffer Layer Enables 1.2 V Open-Circuit Voltage in Cuprous Oxide Solar Cells. *Adv. Mater.* **2014**, DOI: 10.1002/adma.201401054.

(7) Lee, S. W.; Lee, Y. S.; Heo, J.; Siah, S. C.; Chua, D.; Brandt, R. E.; Kim, S. B.; Mailoa, J. P.; Buonassisi, T.; Gordon, R. G. Improved Cu_2O-Based Solar Cells Using Atomic Layer Deposition to Control the Cu Oxidation State at the p−n Junction. *Adv. Energy Mater.* **2014**, *4*, 1301916.

(8) Shinagawa, T.; Onoda, M.; Fariza, B. M.; Sasano, J.; Izaki, M. Annealing Effects and Photoelectric Properties of Single-Oriented Cu_2O Films Electrodeposited on Au(111)/Si(100) Substrate. *J. Mater. Chem. A* **2013**, *1*, 9182−9188.

(9) Tanaka, H.; Shimakawa, T.; Miyata, T.; Sato, H.; Minami, T. Electrical and Optical Properties of TCO-Cu_2O Heterojunction Devices. *Thin Solid Films* **2004**, *469−470*, 80−85.

(10) Musselman, K. P.; Wisnet, A.; Iza, D. C.; Hesse, H. C.; Scheu, C.; MacManus-Driscoll, J. L.; Schmidt-Mende, L. Strong Efficiency Improvements in Ultra-Low-Cost Inorganic Nanowire Solar Cells. *Adv. Mater. (Weinheim, Ger.)* **2010**, *22*, E254−E258.

(11) Fan, J.; Gueell, F.; Fabrega, C.; Shavel, A.; Carrete, A.; Andreu, T.; Ramon, M. J.; Cabot, A. Enhancement of the Photoelectrochemical Properties of Cl-Doped ZnO Nanowires by Tuning Their Coaxial Doping Profile. *Appl. Phys. Lett.* **2011**, *99*, 262102/1−262102/4.

(12) Pauporté, T.; Jouanno, E.; Pellé, F.; Viana, B.; Aschehoug, P. Key Growth Parameters for the Electrodeposition of ZnO Films with an Intense UV-Light Emission at Room Temperature. *J. Phys. Chem. C* **2009**, *113*, 10422−10431.

(13) Izaki, M.; Chizaki, R.; Saito, T.; Murata, K.; Sasano, J.; Shinagawa, T. Hybrid ZnO/Phthalocyanine Photovoltaic Device with Highly Resistive ZnO Intermediate Layer. *ACS Appl. Mater. Interfaces* **2013**, *5*, 9386−9395.

(14) Lupan, O.; Pauporté, T. Hydrothermal Treatment for the Marked Structure and Optical Quality Improvement of the ZnO Nanowire Arrays Deposited on Lightweight Flexible Substrate. *J. Cryst. Growth* **2010**, *312*, 2454−2458.

(15) Goux, A.; Pauporté, T.; Lincot, D. Oxygen Reduction Reaction on Electrodeposited Zinc Oxide Electrodes in KCl Solution at 70°C. *Electrochim. Acta* **2006**, *51*, 3168−3172.

(16) Mandin, P.; Pauporté, T.; Fanouilière, P.; Lincot, D. Modelling and Numerical Simulation of Hydrodynamical Processes in a Confined Rotating Electrode Configuration. *J. Electroanal. Chem.* **2004**, *565*, 159−173.

(17) Izaki, M.; Omi, T. Transparent Zinc Oxide Films Prepared by Electrochemical Reaction. *Appl. Phys. Lett.* **1996**, *68*, 2439−2440.

(18) Elbelghiti, H.; Pauporte, T.; Lincot, D. Mechanistic Study of ZnO Nanorod Array Electrodeposition. *Phys. Status Solidi A* **2008**, *205*, 2360−2364.

(19) Pauporté, T.; Bataille, G.; Joulaud, L.; Vermersch, F. J. Well-Aligned ZnO Nanowire Arrays Prepared by Seed-Layer-Free Electrodeposition and Their Cassie-Wenzel Transition after Hydrophobization. *J. Phys. Chem. C* **2010**, *114*, 194−202.

(20) Chastain, J. *Handbook of X-ray Photoelectron Spectroscopy;* Perkin-Elmer Corporation: Waltham, MA, 1992.

(21) Klein, J. C.; Hercules, D. M. Surface Characterization of Model Urushibara Catalysts. *J. Catal.* **1983**, *82*, 424−441.

(22) Shinagawa, T.; Ida, Y.; Mizuno, K.; Watase, S.; Watanabe, M.; Inaba, M.; Tasaka, A.; Izaki, M. Controllable Growth Orientation of Ag_2O and Cu_2O Films by Electrocrystallization from Aqueous Solutions. *Cryst. Growth Des.* **2013**, *13*, 53−58.

(23) Mora-Sero, I.; Fabregat-Santiago, F.; Denier, B.; Bisquert, J.; Tena-Zaera, R.; Elias, J.; Levy-Clement, C. Determination of Carrie Density of ZnO Nanowires by Electrochemical Techniques. *Appl. Phys. Lett.* **2006**, *89*, 203117/1−203117/3.

(24) Rousset, J.; Saucedo, E.; Lincot, D. Extrinsic Doping of Electrodeposited Zinc Oxide Films by Chlorine for Transparent Conductive Oxide Applications. *Chem. Mater.* **2009**, *21*, 534−540.

(25) Shinagawa, T.; Chigane, M.; Murase, K.; Izaki, M. Drastic Change in Electrical Properties of Electrodeposited ZnO: Systematic Study by Hall Effect Measurements. *J. Phys. Chem. C* **2012**, *116*, 15925−15931.

(26) Chen, J.-W.; Perng, D.-C.; Fang, J.-F. Nano-Structured Cu_2O Solar Cells Fabricated on Spare ZnO Nanorods. *Sol. Energy Mater. Sol. Cells* **2011**, *95*, 2471−2477.

(27) Joint Committee on Powder Diffraction Standards. *Powder Diffraction File;* International Centre for Diffraction Data: Newtown Square, PA, 1992; pp 41−1445.

(28) Joint Committee on Powder Diffraction Standards. *Powder Diffraction File;* International Centre for Diffraction Data: Newtown Square, PA, 1992; pp 36−1451.

(29) Joint Committee on Powder Diffraction Standards. *Powder Diffraction File;* International Centre for Diffraction Data: Newtown Square, PA, 1992; pp 5−667.

(30) Guérin, V. M.; Pauporté, T. From Nanowires To Hierachiral Structures of Template-Free Electrodeposited ZnO for Efficient Dye-Sensitized Solar Cells. *Energy Environ. Sci.* **2011**, *4*, 2971−2979.

(31) Musselman, K. P.; Marin, A.; Wisnet, A.; Sheu, C.; MacManus-Driscoll, J. L.; Schmidt-Mende, L. A Novel Buffering Technique for Aqueous Processing of Zinc Oxide Nanostructures and Interfaces, and Corresponding Improvement of Electrodeposited ZnO-Cu_2O Photovoltaics. *Adv. Funct. Mater.* **2011**, *21*, 573−582.

(32) Luqua, A.; Marti, A. Chapter 4. In *Handbook of Photovoltaic Science and Enineering;* Luqua, A., Hegedus, S., Eds.; Wiley: Chichester, West Sussex, 2003; pp 120−124.

(33) Sze, S. M.; Ng, K. K. *Physics of Semiconductor Devices,* 3rd ed; Wiley: Hoboken, NJ, 2007.

(34) Terada, N.; Widodo, R. T.; Itoh, K.; Kong, S. H.; Kashiwabara, H.; Okuda, T.; Obara, K.; Niki, S.; Sakurai, K.; Yamada, A.; Ishizuka, S. Characterization of Interface Nature and Band Alignment in CBD-

CdS/Cu(In,Ga)Se_2 Bi-Layer Structure by Photoemission and Inverse Photoemission Spectroscopy. *Thin Solid Films* **2005**, *480−481*, 183−187.

(35) Minami, T.; Nishi, Y.; Miyata, T.; Nomoto, J. High-Efficiency Oxide Solar Cells with ZnO/Cu_2O Heterojunction Fabricated on Thermally Oxidized Cu_2O Sheets. *Appl. Phys. Express* **2011**, *4*, 062301/1−062301/3.

(36) Nishi, Y.; Miyata, T.; Minami, T. The Impact of Heterojunction Formation Temperature on Obtainable Conversion Efficiency in N-ZnO/P-Cu_2O Solar Cells. *Thin Solid Films* **2013**, *528*, 72−76.